Study on Degradation of Solid Oxide Fuel Cell Anode by using pure Ni Electrode

Zhenjun Jiao[a], Naoki Shikazono*[a], Nobuhide Kasagi[b]

a. Institute of Industrial Science, University of Tokyo 4-6-1 Komaba, Meguro-ku, Tokyo. 153-8505, Japan

b. Department of Mechanical Engineering, University of Tokyo, Bunkyo-ku, Tokyo 113-8656, Japan

Abstract

In this study, the interactions between Ni and YSZ in solid oxide fuel cell anode and the influence of glass seal to anode performances have been investigated by using screen-printed pure Ni anode sintered on YSZ pellet. The evolution of Ni-YSZ interface in 100 hours galvanostatic polarization in hydrogen is studied with different humidities in hydrogen. Compared with conventional Ni-YSZ composite cermet anode, this method has the advantage of direct observation at Ni-YSZ interface where degradation takes place. Electrochemical impedance spectroscopy was applied to analyze the time variation of the anode electrochemical characteristics. The interface microstructural changes were characterized by scanning electron microscopy. The influence of bulk gas humidity, gas-sealing material and Ni coarsening on anode durability was studied. The degradation of pure Ni anode is considered to be determined by the competition among the mechanisms of silicon deposition, YSZ interface morphological change and Ni coarsening.

Key words: SOFC, TPB, silicon, zircon, interface ;

1. Introduction

Solid oxide fuel cell (SOFC) has been attracting more and more attentions in the last few decades as an attractive energy conversion device. SOFC has the advantages such as fuel flexibility and high efficiency [1]. The current challenge focuses on the long-time stability and durability of SOFC electrodes. In the industrial applications, a durability of more than $40,000$ hrs is expected, while most current SOFC anodes exhibit significant degradation in long time discharge experiments, which is after caused by the coarsening of Ni [2, 3]. With higher current density or overpotential, rapid degradation or even sudden failure of the cell can be observed [4].

Email address: shika@iis.u-tokyo.ac.jp (Naoki Shikazono*[a])

Simwonis et al. [5] studied the coarsening of Ni particles in porous anode and correlated the changes in electrical conductivity with the microstructural parameters. A large decrease in electrical conductivity was observed in 4000 hrs exposure in humidified hydrogen without discharge, which can be explained by the increase of average Ni particle size from 2 μm to 2.6 μm. Koch et al. [2] tested SOFC performance and degradation under several operating conditions. A critical anode-cathode voltage was found, below which the degradation rate was significant. The same result has also been proven by Matsui et al. [4], and at the same time, the influence of fuel humidity was observed to be significant on the performance and stability of Ni-YSZ cermet anode. In their experiments, sudden failure of the cell was observed when the fuel humidity was 40%. Rapid micro-structure change of Ni was observed. It was concluded that some factors other than the morphological changes of Ni in the composite anode cause the degradation or even sudden death of the SOFC anode. The possible reasons can also be attributed to the local degradation at three phase boundary (TPB, hereafter) caused by impurities accumulation. However, no systematic studies were conducted to specify the interactions between Ni and YSZ in these studies. In order to further investigate the interactions between Ni and YSZ phases, Hansen et al. [6] studied the Ni-YSZ interaction along TPB by using Ni wire as a simplified anode. A film of impurities was found at Ni-YSZ interface while impurity ridges were also found to accumulate along TPB. At the same time, impurity glass phase was found to form hill and valley structures in sub-micron scale at the contacting area. Several kinds of impurities were found in the ridge along TPB, which made the local reaction even more complex. In order to elucidate the reaction mechanism with pure Ni, Mizusaki et al. [7, 8] employed Ni stripe pattern electrodes prepared on the surface of YSZ with well defined morphology. The rate of anodic reaction was found to be determined by the reaction of hydrogen and the absorbed oxygen on Ni surface. From the literature [7, 9, 10], it can be concluded that the long-period degradation of Ni-YSZ cermet anode is due to Ni migration [2, 11, 12] which causes the disconnection of Ni network. Systematical work has been conducted by Jiao et al. [13] to study the local morphological changes of Ni by using mechanically pressed porous Ni pellet as an anode. However these papers studied mechanical pressed or deposited pure Ni anodes without considering the sintering effect on Ni-YSZ interface.

Degradation of conventional Ni-YSZ composite anode includes complicated processes, parameters and phenomena, which cannot be explained only by a simple Ostwald ripening mechanism [14]. There are other mechanisms causing complex interplay between Ni and YSZ at their interface [15, 16], such as Ni volatilization [13] and the microstructural reorganization of both Ni [8, 17] and YSZ [6]. In this paper, high purity NiO was screen-printed and sintered onto commercial YSZ electrolyte pellet, after which it was

reduced and employed as anode and operated at 800^{o}C. Glass is a popular material used for gas-sealing in SOFCs systems, which is considered as the main source of impurities in this study. The study focuses on the influences of impurity phase and microstructual changes at Ni-YSZ interface, while similar processes can happen in conventional composite Ni-YSZ anode to cause degradation [18]. Compared to conventional Ni-YSZ composite anode, the new method has the advantage of easy observation of the reaction sites, which facilitates the correlation between Ni-YSZ interactions and anode performance.

2. Experimental materials and devices

NiO powder (AGC Seimi Chem. Corp., Japan) used in this study has an average particle diameter of 1.1μm with high purity ($>$ 99.9 mol%). The powder was mixed with terpineol solvent and the ethylcellulose binder in agate mortar to obtain anode screen-printing slurry. The slurry was screen-printed onto commercial dense 8mol% YSZ pellet (diameter 20 mm, thickness 0.5 mm, Fine Ceramics Corp., Japan) with a diameter of 10 mm and then sintered at 1400^{o}C for 3 hours to obtain a strong bonding between YSZ and NiO. About 0.13 mol% Mg has been detected as the main impurity component in YSZ.

$(La_{0.8}Sr_{0.2})_{0.97}MnO_3$ (LSM) powder (0.4μm) mixed with YSZ powder (0.1μm) in a mass ratio of 1 : 1 was used as a cathode material. The powder was mixed with terpineol solvent and ethylcellulose binder in agate mortar to obtain cathode printing slurry. The slurry was screen-printed onto the counter side of the commercial YSZ pellet with a diameter of 10 mm as a cathode. The cathode was sintered at 1200^{o}C for 3 hours.

The details of SOFC performance measurement setup has been described in the previous paper [13]. The YSZ pellet was surrounded by a Pt wire as reference electrode. Pt paste was used to enhance the conductive connection between Pt wire and YSZ pellet. Nitrogen was introduced as protective gas in the initial heating up stage. After the furnace temperature had been raised up to 700^{o}C, glass seals completely melted over the edges of the cell, the reference electrode and the two outer tube edges, which resulted in good sealing. Then, dry hydrogen was introduced for 1 hour to reduce NiO. The performance of SOFC was evaluated at 800^{o}C by using humidified hydrogen as a fuel and pure oxygen as an oxidant (50 mlmin^{-1} for both anode and cathode). Cell impedance spectra (frequency range: $1 - 10^5$ Hz, AC signal strength: 10 mV) measurements were conducted with a Solatron frequency analyzer (1255B) and a Solatron interface via current collectors. The software Zplot/Zview was used to monitor and control the hardware to analyze

impedance spectroscopy. Anode-reference static current method was applied to test the cell anode durability.

Two different long time measurement programs have been conducted:

1. Anodes are discharged in hydrogen with different humidities, with a constant current density of 200 $mAcm^{-2}$ for 100 hours.
2. Anodes are kept at OCV in hydrogen with different humidities for 100 hours.

The observations of the sample microstructures were facilitated by FIB-SEM (Carl Zeiss, NVision40). The secondary electron images of Ni surface were obtained by a chamber detector and YSZ surface by an in-lens detector. The elemental analysis was conducted by energy dispersive X-ray spectroscopy (EDX; Thermo Electron, NSS300). Every discharge experiment had been repeated several times to confirm the reproducibility of the experimental results.

3. Experimental results

3.1. Anode performances in different humidities

Four humidities, dry, 3%H_2O, 10% H_2O and 30% H_2O, were applied at anode in the discharging experiments. Figure 1 shows the transient performances of four anodes. It can be seen that the performance curves under dry, 3% H_2O and 10% H_2O conditions presented various degradation rates from the beginning of discharge to the end. The anode degradation rates in dry hydrogen and 30% H_2O hydrogen were higher than in 3% H_2O and in 10% H_2O hydrogen. For the anode tested in dry hydrogen, its degradation rate decreased with time and the performance reached a relatively stable state after about 80 hours. For the anode tested in 30% H_2O hydrogen, a sudden failure was observed after about 20 hours operation. Anodes tested in 3% H_2O hydrogen and 10% H_2O hydrogen went through relatively stable stages initially and the stable stage lasted longer in higher humidities. After the initial stable discharge stage, a relatively slower degradation rate was observed for both cases.

In order to investigate the Ni-YSZ interface degradation mechanism, the anode-reference impedance evolutions with and without discharge were compared. 3%H_2O hydrogen was chosen as the standard testing environment. Figure 2 shows the anode-reference impedance changes against time when the anode was kept at OCV for 100 hours. It can be seen that both the ohmic resistance and polarization impedance kept increasing with time. After 100 hours, the ohmic impedance increased from about 0.86 Ω to 1.03 Ω,

with an average degradation rate of 0.0017 $\Omega hour^{-1}$. The polarization impedance increased from less than 10 Ω to about 450 Ω. Figure 3 shows the anode-reference impedance changes against discharge time within 100 hours. It can be seen that the ohmic resistance kept increasing, similarly as in OCV situation from about 0.79 Ω to 0.93 Ω, with an average degradation rate of 0.0014 $\Omega hour^{-1}$. The polarization impedance increased initially and started to decrease from about 10 hours until the end of the test.

3.2. Microstructure changes

3.2.1. After discharge

Figure 4 (a) show the top-views of anode after reduction that no Ni delamination was observed when the samples were cooled down to room temperature. The later scratching test further proved the strong bonding remained between Ni and YSZ. Figures 4 (b)-(e) show the top-views of anode after 100 hours discharge in different humidities corresponding to Fig. 1 (a)-(d). After 100 hours discharge, the electrolyte surface color became dark compared to the original YSZ pellet, especially for dry hydrogen case. The dark color presented a gradient from the edge of the anode outwards. The pure Ni anodes tested in dry, 3% H_2O and 10% H_2O hydrogen were partially delaminated off from the electrolyte substrate. For 30% H_2O case, the anode was almost totally delaminated off from YSZ pellet which can explain the sudden failure of anode around 20 hours that all active TPB became de-active because of the lost contact between Ni and YSZ.

Figure 5 shows Ni-YSZ interfaces after reduction and discharge in different humidities, while Ni had been mechanically removed from YSZ surface. After reduction, on YSZ surface, only the NiO-embedded pattern formed during the high temperature sintering can be observed, with the Ni-contacting YSZ surface remained smooth. Certain residual independent Ni particles were bonded to YSZ surface with a round shape. After four discharge experiments, a morphologically-modified interface can be observed at YSZ surface which used to contact with Ni. After anode discharge in dry hydrogen for 100 hours, a smooth interlayer was observed between Ni and YSZ with a clear accumulation ridge. With the increase of humidity, the Ni-contacting YSZ interface become rough and the ridge-rim became unclear and disappeared when the humidity became 10%. In 30% H_2O case, the anode presented a sudden failure after about 20 hours discharge, while the Ni-contacting interface was smoother than 3% H_2O and 10% H_2O cases, which may be due to the short discharge time. Besides the interface region, certain amount of independent satellite droplets were observed surrounding the interface in dry case and the amount decreased with the increase of humidity, and no droplets were observed in 10% H_2O case. In 30% H_2O case, smaller independent droplets were observed surrounding

the interface with different morphologies. Since the sizes of both the interface region and the independent droplets were beyond the resolution of EDX mapping, point-EDX was used to identify the content of interface and the independent droplets, qualitatively. Figure 6 shows the point-EDX spectra which corresponds to the positions red cross symbols in Fig. 5(b)-(e). The main elements of the interlayer in dry hydrogen were identified to be Zr, Si, Mg, C, Y and O. Zr, C, Y and O were identified for the other three cases. With the increase of humidity, the amount of Si and Mg decreased dramatically. Carbon was pre-coated to prevent the charging effect in SEM imaging process. Silicon was also detected which is considered to be mainly in SiO_2 state, especially in dry hydrogen case. Liu et al. [19] have applied FIB/lift-out techniques to TEM specimen preparation of an anode-electrolyte interface from a long-term tested Ni-YSZ half-cell, allowing the interfacial microstructure to be analyzed on nano-scale. Their work found that a very small amount of SiO_2, which originates from raw materials degrades the anode-electrolyte interface and Ni-YSZ grain boundaries by forming nanometer-thin silicate glass films after long-term discharge. In this study, the formation of SiO_2 droplets suggests that the silicon accumulation was not just caused by the segregation of materials impurities as reported, but also caused by the other silicon impurity source. In this study, small amount of other elements such as Al and Na, in addition to the previously mentioned Mg, which can compose alkali silicate glass phase. The independent droplets observed around the Ni-contacting area in dry and 3% H_2O cases were identified to be SiO_2 droplets. The smaller size independent droplets in 30% H_2O case around the interface were identified to be Ni droplets.

3.2.2. After kept at OCV

As shown in Fig. 7, the Ni-contacting YSZ interfaces without discharge were found to be clear, and no obvious morphological change was observed in all humidities. The YSZ surface morphology kept almost the same as just after reduction. Besides, in OCV experiments, no dark color change was observed on free YSZ surface after 100 hours in four humidities. From the comparison to Fig. 5 (b)-(e), it can be proven that the interlayer formed in dry hydrogen and YSZ surface morphological changes took place only during discharging processes.

4. Discussions

4.1. Morphological changes of Ni-YSZ interface

It has been reported that the bonding strength between YSZ and NiO after high temperature sintering is stronger than that between YSZ and Ni after the subsequent reduction of Ni [20, 21]. In high temperature

sintering, molten nickel-oxygen eutectic mixture can be formed and a good contact between NiO and YSZ phases can be obtained. The stress caused by thermal expansion mismatching between NiO and YSZ can be released due to the YSZ surface pattern formation during sintering and the presence of liquid phase which wets the interface well. Upon solidification of the eutectic melt, a strong bond can be established. After reduction, the strong bond based on the eutectic layer disappears as shown in Fig. 8. A clear boundary can be observed between two phases and certain inter-pore and gap were formed. Similar phenomena has been reported by Jeangros et al. [22]. During the experiments, anode was reduced at high temperature and kept nearly unchanged in discharge operation that the thermal expansion coefficients mismatching between Ni and YSZ can not dominate the delamination of Ni. As shown in Fig. 4 (a), cooling process of the reduced anode to room temperature did not result in significant Ni delamination. Thus, it is considered that the delamination can be attributed to the discharging process.

Glass ring used in our experiment is made of 75% SiO_2, and Na, Ca silicates. SiO_2 can be corroded by hydrogen at high temperatures and produces gaseous SiO through reaction (1) [23, 24].

$$SiO_{2(s)} + H_{2(g)} \rightleftharpoons SiO_{(g)} + H_2O_{(g)} \tag{1}$$

Gaseous SiO is not stable and it is decomposed rapidly. The composition of deposited independent droplets around interface area observed in Fig. 5 (b)(c) were considered to be a mixture of Si and SiO_2 formed by reaction (2).

$$2SiO_{(g)} \rightleftharpoons SiO_{2(s)} + Si_{(s)} \tag{2}$$

In dry hydrogen case, the deposition of Si on free YSZ surface may explain the dark color coating phenomena as shown in Fig. 4 (b). At the same time, with the presence of ZrO_2 in YSZ, stable zircon ($ZrSiO_4$) can be produced in a reduction environment, as shown in reaction (3).

$$2SiO_{(g)} + ZrO_{2(s)} \rightleftharpoons ZrSiO_{4(s)} + Si_{(s)} \tag{3}$$

The rare-earth oxide, like Y_2O_3, and impurities can react as mineralizer (material which catalyzes the reaction) in reaction (3) [25]. The deposited SiO_2 can then be stabilized by producing stable zircon layer on YSZ surface. Eppler et al.[26, 27] have demonstrated that an oxygen atmosphere is not necessary for the formation of zircon. The reaction mechanism is the same as zircon formation in air. Besides, humidity either

produced by electrochemical reaction in discharge or brought in by inlet hydrogen, can favor the formation of zircon [27]. The produced zircon with pigment may also contribute to the dark color coating on YSZ, especially for YSZ surface under Ni phase, as this area always become darker after discharge in different humidities. The zircon produced may enhance the bonding between SiO_2 and YSZ, which can explain the phenomena that the interlayers and accumulated SiO_2 droplets were bonded strongly to YSZ surface even after cooling down of the cell.

The long term stability of 8mol% YSZ material at SOFC operating temperature has been investigated, where a significant aging effect of the material conductivity was observed after 1000 hours annealing at 1000^oC [1, 28]. In this study, the long-time aging effect of YSZ may contribute to the increase of ohmic resistance, but can not dominate the process since the temperature is low and the annealing time is short. Rodrigues et al. [29] have reported that in high temperatures or long-period thermal treatments, yttrium can be displaced from the electrolyte to glass phase, which can cause zirconia crystal transformation with the decrease of ionic conductivity and the mechanical disruption of the YSZ surface.

Butz et al. [30] reported that 8YSZ was not fully stabilized in the cubic phase, while the material contained nanoscale regions of metastable tetragonal crystal phase, which are coherently embedded in the cubic phase YSZ. Badwal [3, 31] and Sato et al. [32] have reported that the tetragonal-monoclinic crystal structure transformations and the change of microstructure resulting from low-temperature annealing of YSZ in humidity were much greater than those observed in dry atmosphere. It is known that the local humidity concentration at active TPB can be much higher than that in bulk gas in discharge [13, 33, 34]. The YSZ kept losing its ionic conductivity with the degradation process caused by tetragonal-monoclinic crystal transformation, which may explain the increase of ohmic resistance, since the contribution of pure Ni to ohmic resistance can be ignored. In pure Ni anode, active TPBs distribute on a 2D YSZ surface with much smaller TPB length compared to conventional Ni-YSZ composite anode. Thus, the local humidity can be very high because of higher local current density for a fixed total current value. This increased local humidity then accelerates YSZ crystal transformation and finally modifies the YSZ surface morphology in a rather short period at active TPB vicinity, which can be easily observed by SEM. Quantitative study should be conducted in the future by applying X-ray photoelectron spectroscopy method. At the Ni-YSZ contacting interface, active TPB was not uniformly distributed along the contacting area edge because of porous reduced Ni phase as shown in Fig. 8 (b). This leads to a non-uniform local humidity distribution,

which results in non-uniform crystal structure transformation and then the rough YSZ surface.

The equilibrium partial pressures of different gaseous phases were calculated by chemical thermodynamics software FactSage and plotted against humidity in Fig. 9. Gaseous SiH_4 can be ignored in humidified hydrogen cases in this study as its partial pressure is several order lower than SiO. The deposition of SiH_4 is considered to be significant only in dry hydrogen case when unstable SiH_4 can easily decompose into solid Si and hydrogen. The decompositions of SiH_4 and SiO made the YSZ surface much darker than the other three cases in humidified hydrogen. The deposition effect was favored by high humidity which led to the outward gradation of the dark color from at the anode edge, since the region near anode experienced higher humidity produced in the discharging process. As the local humidity concentration at active TPB can be much higher than bulk gas in discharge, the humidity gradient from local TPB to bulk can drive gaseous SiO diffusion (plus SiH_4 in dry hydrogen case) from bulk towards TPB vicinity. Thus, solid SiO_2 and Si deposit around TPBs. The transport of gaseous silicon, followed by the diffusion of silicon and oxygen across the zircon product layer to a reaction site on YSZ can enhance reaction (3) [25–27]. It is known that viscosity of a silica glass drops significantly with the increase of humidity and the presence of certain impurities [19]. With a high wettability and mobility, the glass phase forms films at the Ni-YSZ grain boundaries which was observed as an interlayer in dry hydrogen case. The glass phase interlayer at the same time served as paths of high mobility required for the impurities to segregate and accumulate to the Ni-YSZ interface, which explains the EDX spectra peak of Mg in dry hydrogen case. At SOFC operation temperature, the liquid glass phase formed by the deposition of SiO and the segregated impurities can penetrate into the gap between Ni and YSZ formed during reduction process as shown in Fig. 8 (b). When the gaps are fully filled, SiO and impurities accumulate along the edge of the interface. The interlayer and accumulation ridge can partially block the active TPB [6, 35], which results in the increase of anode ohmic resistance and a relatively fast anode degradation.

With the increase of bulk gas humidity, the interface degradation mechanism is changed as the gaseous SiO concentration in bulk gas decreases by several orders. The reduced concentration of gaseous SiO in bulk gas explains the disappearance of visible glass phase interlayer, the independent silicon content droplets and the dark color on the YSZ surface. In 3% H_2O, 10% H_2O and 30% H_2O cases, small amount of Si still can be detected by point-EDX as shown in Fig. 6, which indicates that glass phase may still exist at Ni-YSZ interface with an invisible thickness. In dry hydrogen case, because of the complete coverage of silica and

relatively lower local humidity, the modification of YSZ surface was prohibited. Besides, the coverage of glass phase promoted the uniform distribution of impurities so that no obvious rough interface was observed. When the bulk gas humidity is high enough, as the 30%H_2O case, an insulation film of zircon may be formed, which completely covers the YSZ surface and results in the sudden failure of anode as shown in Fig. 1 (d). Because of the shorter discharge time, no obvious rough interface was observed in Fig. 5 (e). However, the interface had been morphologically modified in certain extent.

In addition to the accumulation effect of silicon and the modification of YSZ at interface, the coarsening of Ni phase is another mechanism causing the anode degradation which has been widely studied in literature [1, 13]. The coarsening of Ni phase results in the weakening of Ni-YSZ contact [36], especially for pure Ni anode which is without the alleviation of YSZ skeleton as conventional composite Ni-YSZ anode. The loss of Ni-YSZ contact contributed to the anode degradation and the final delamination of Ni from YSZ after all the experiments. In humidified hydrogen, the sintering rate of Ni can be hundred times accelerated than in dry hydrogen [14–16, 37], which explains the increased delamination rate of Ni with the increase of bulk gas humidity. Besides, gaseous SiO can also react with Ni surface and form Ni silicide in hydrogen as shown in reaction (4). The formation of Ni silicide may also influence Ni sintering process by changing the surface diffusion of Ni.

$$2\mathrm{SiO}_{(g)} + x\mathrm{Ni}_{(s)} \rightleftharpoons \mathrm{Ni}_x\mathrm{Si}_{(s)} + \mathrm{SiO}_{2(s)} \tag{4}$$

At high temperature, Ni silicide has been reported to be unstable. The nucleation of Ni silicide occurs above 750^{o}C [38], which leads to the aggregation of silicide. The presence of Ni silicide aggregation island on Ni surface may influence the Ni surface diffusion rate and the Ni network sintering rate. As the mechanism of Ni silicide formation and its influence to Ni sintering rate is out of the range of this paper, the details will be investigated in the future work.

With the increase of humidity, Ni phase can also vaporize as volatile $Ni(OH)_2$ as shown in reaction (5) [13].

$$\mathrm{Ni}_{(g)} + 2\mathrm{H}_{2(g)}\mathrm{O} \rightleftharpoons \mathrm{Ni(OH)}_{2(g)} + \mathrm{H}_{2(g)} \tag{5}$$

The partial pressures of gaseous SiO and SiH_4 decrease with the increase of humidity, while the partial

pressure of gaseous $Ni(OH)_2$ increase and exceed SiO concentration when humidity is higher than 1%. The vaporization-deposition mechanism of gaseous $Ni(OH)_2$ driven by humidity gradient near active TPB can explain the deposition of small Ni droplets as shown in Fig. 5(e), which has been reported in Ref. [13].

4.2. Correlation of interface morphological changes to anode performance

The increase of ohmic resistance in SOFC anode is considered to be caused by the loss of electrode-electrolyte contact or by the formation of contamination interlayer [1], and the increase of polarization impedance is due to the decrease of active TPB density [1, 17]. Since there is no YSZ skeleton to prevent Ni coarsening, pure Ni anode is much less durable than composite anode. Figure 2 shows the negative effect of Ni coarsening on the Ni-YSZ interface durability without the influence of discharge. The reason that can explain the increase of both ohmic resistance and polarization impedance is that Ni phase was delaminated continuously off YSZ surface. Delamination was due to the mechanical stress formed by the shrinkage of Ni network in coarsening process. In OCV, gaseous silicon was kept at equilibrium state without deposition as there was no humidity gradient. Compared to the negative effect of delamination, Figure 3 shows the positive effect of discharge on Ni-YSZ interface durability. The roughening morphological change of YSZ surface resulted in an increase of active TPB density. The increase of polarization impedance caused by Ni delamination is then fully compensated.

The compensation mechanism can explain the initial stable performance for 3% H_2O and 10% H_2O hydrogen cases. The increase of ohmic resistance is compensated by the decrease of polarization impedance. In dry hydrogen case, a relatively fast degradation rate was observed which can be explained by the non-conductive glass phase interlayer and accumulated ridge, which partially blocked the active TPB so that the reducing polarization impedance can not fully compensate the degradation rate. In 30% H_2O hydrogen case, high humidity enhances reaction (3) and forms insulation film of zircon which may explain the sudden failure of the anode.

4.3. Further study on pure Ni anode degradation by using gold for gas-sealing

Based on the current experimental data, it is not sufficient to prove the assumed mechanisms of silicon deposition and zirconia crystal structure transformation described above. In order to further investigate the Ni-YSZ interface degradation mechanism, another three experiments were conducted within dry, 3% H_2O

and 30% H_2O hydrogen, with gold as gas-sealing material. All other conditions were kept unchanged for comparison.

Figure 10 shows the transient performances of the three anodes in 100 hours discharge and the corresponding top-view images of anodes after the experiments. It can be seen that the performance curves under dry, 3% H_2O and 30% H_2O conditions presented very different degradation rates compared to Fig. 1 (a)(b)(d). The anode degradation rates in dry and 30% H_2O hydrogen are larger than in 3% H_2O hydrogen in the initial 20 hours. The degradation terminated in the three tests and led to general stable performances until the end of the test. For 30% H_2O case, a small increase of performance can be observed after 50 hours. No sudden failure of anode was observed within 100 hours operation and a periodic oscillating performance appeared after about 72 hours discharge until the end of the test. The three cells remained white color without becoming dark.

Figure 11 shows the YSZ-Ni interfaces after discharge corresponding to Fig. 10. When the anode was discharged in dry hydrogen for 100 hours with gold seal, a smooth interface can be observed without an impurity interlayer or accumulated ridge. Some small-size particles were bonded to the interface which were hardly identified by EDX. With the increase of humidity, the Ni-contacting interface become rough as was seen in glass seal experiments. This eliminates the influence of glass phase on the YSZ surface modification, while the crystal transformation might be dominated by the influence of high local humidity which deserves further investigation. For all the three samples, no independent satellite droplets around interface were observed. Compared to Fig. 5, very different morphological change was observed for dry and 30% H_2O hydrogen cases. Figure 12 shows the anode-reference impedance changes after different discharge times in 3% H_2O with gold seal. It is seen that the ohmic resistance kept increasing from about 0.75 Ω to 0.99 Ω, with an average degradation rate of 0.003 Ωhour^{-1}, about twice of the result of glass seal test. The decrease of polarization impedance can compensate the increase of ohmic resistance. The higher degradation rate of ohmic resistance in gold seal experiments can be explained by the absence of Ni silicide caused by reaction (4). Figure 13 shows the top surface of anode after reduction, exposed in dry hydrogen for 100 hours by applying both glass and gold seals. Compared to reduced Ni, it can be clearly seen that, totally different sintering processes were observed under the same environment. Although the Ni sintering at Ni-YSZ interface might be different from that at the top surface of anode, the influence of gaseous silicon species has been validated. It can be derived from the decrease of polarization impedance that the local active TPB

density was enhanced by certain mechanism in discharge. Point-EDX method had been used to measure the YSZ interface area, while no significant signal of silicon was detected.

4.4. Dissusion for glass seal and gold seal results

The performance differences between glass seal and gold seal experiments can be explained by the influence of silicon deposition at TPB and its influences to the bulk Ni sintering process. In dry hydrogen, with glass seal, larger amount of silicon deposition formed glass interlayer at TPB and the surrounding independent silica droplets. The glass phase partially blocks the active TPB and results in a rather fast degradation. With the increase of bulk gas humidity, the silicon deposition still took place but it was prohibited by the drastic reduction of gaseous SiO concentration in bulk gas. Simultaneously, the tetragonal-monoclinic phase transformation of zirconia and the production of zircon were favored by the local high humidity near TPB, which led to the morphological change of Ni-YSZ interface and the loss of YSZ ionic conductivity. When the humidity was higher than a critical value, an zircon insulation layer can be formed to cause the sudden failure of anode. When gold seal was applied, the Ni-YSZ interface degradation was only dominated by Ni coarsening and the YSZ phase change which were enhanced by high local humidity at TPB. No interlayer or insulation film can be formed without the deposition effect of gaseous silicon species, so that the anode performances were obviously improved compared to glass seal cases.

The interfaces morphology comparison between glass seal and gold seal experiments clearly validates the influences of silicon to the anode performances. The most obvious differences were observed in two extreme humidity conditions: dry and 30% H_2O hydrogen. In dry hydrogen discharge process with glass seal, glass phase interlayer, accumulation ridge and independent droplets can be clearly observed around TPB, while they all were not observed in gold seal experiments. The anode always experienced a sudden failure in 30% H_2O hydrogen discharge process with glass seal, while no such sudden failure was observed with gold seal. Instead, a periodic oscillation was observed, which may be explained by a periodic building-up-releasing cycle of local stress tension at Ni-YSZ interface caused by the vaporization-deposition cycle of $Ni(OH)_2$ [6, 13]. The reason of larger increasing rate of ohmic resistance in gold seal experiments for 3% humidity case is not clear so far. The possible reason might be the influence of Ni silicide on Ni sintering processes shown in Fig. 13, which deserves a further investigation in the future.

The competition among the three mechanisms, , i.e., silicon species deposition, YSZ interface morphological change and the coarsening of Ni phase, finally determines the anode performance and durability. In conventional Ni-YSZ composite anode, the similar Ni-YSZ interface degradation mechanisms should take place if glass ring is used for gas-sealing. Gold is proposed to be a better choice for gas-sealing material to get rid of the influence of silicon deposition. The mechanism of YSZ crystal transformation at TPB in discharging process also needs to be further investigated.

5. Conclusions

In this study, pure Ni anode was applied to study the degradation mechanisms at Ni-YSZ interface instead of conventional Ni-YSZ composite anode. In the anode discharging process, three mechanisms, i.e., silicon deposition at TPB, zirconia crystal structure transformation and the coarsening of bulk Ni, take place simultaneously with glass used as the gas-sealing material. The silicon deposition mechanism can cause the accumulation of glass phase at TPB, which can partially block the active TPB and result in a fast anode degradation. The local high humidity generated by electrochemical reaction at active TPB can enhance the local zirconia crystal transformation, which leads to the loss of YSZ conductivity and the morphological change of Ni-YSZ interface. For very high bulk gas humidity, accelerated Ni sintering and the production of zircon may form insulation film and result in the sudden failure of the anode. The degradation mechanisms can be compensated by the morphological change of Ni-YSZ interface while the rough surface can enhance the local TPB density and reduce the polarization impedance. The competition among the three mechanisms finally determines the pure Ni anode performance and durability. The degradation caused by silicon deposition mechanism can be avoided if gold seal is applied that the anode durability can be obviously improved compared to glass seal experiments.

Acknowledgments

This work was supported by the New Energy and Industrial Technology Development Organization (NEDO) under the Development of System and Elemental Technology on Solid Oxide Fuel Cell (SOFC) Project.

References

[1] S. C. Singhal, K. Kendall, High Temperature Solid Oxide Fuel Cells: Fundamentals, Design and Applications, Elsevier Advanced Technology, 2003.

[2] S. Koch, P. V. Hendriksen, M. Mogensen, Y.-L. Liu, N. Dekker, B. Rietveld, B. D. Haart, F. Tietz, Fuel Cells 2 (2006) 130–136.

[3] S. P. S. Badwal, M. J. Bannister, R. H. J. Hannink, Science and Technology of Zirconia V, Technomic publishing Company, 1993.

[4] T. Matsui, R. Kishida, J.-Y. Kim, H. Muroyama, K. Eguchi, J. Electrochem. Soc. 157 (2010) B776–B781.

[5] D. Simwonis, F. Tietz, D. Stover, Solid State Ionics 132 (2000) 241–251.

[6] K. V. Hansen, K. Norrman, M. Mogensen, J. Electrochem. Soc. 151 (2004) A1436–A1444.

[7] J. Mizusaki, H. Tagawa, T. Saito, T. Yamamura, K. Kamitani, K. Hirano, S. Ehara, T. Takagi, T. Hikita, M. Ippommatsu, S. Nakagawa, K. Hashimoto, Solid State Ionics 70-71 (1994) 52–58.

[8] A. Utz, H. Stormer, D. Gerthsen, A. Weber, E. Ivers-Tiffee, Solid State Ionics 192 (2011) 565–570.

[9] B. de Boer, Hydrogen oxidation at porous nickel and nickel/yttria-stabilised zirconia cermet electrodes, Ph.D. Thesis, University of Twente, The Netherlands, 1998. .

[10] J. Mizusaki, H. Tagawa, T. Saito, K. Kamitani, T. Yamamura, K. Hirano, S. Ehara, T. Takagi, T. Hikita, M. Ippommatsu, S. Nakagawa, K. Hashimoto, J. Electrochem. Soc. 141 (1994) 2129–2134.

[11] M. Brown, S. Primdahl, M. Mogensen, J. Electrochem. Soc. 147 (2000) 475–485.

[12] M. S. Schmidt, K. V. Hansen, K. Norrman, M. Mogensen, Solid State Ionics 180 (2009) 431–438.

[13] Z. Jiao, N. Takagi, N. Shikazono, N. Kasagi, J. Power Sources 196 (2010) 1019–1029.

[14] L. Holzer, B. Iwanschitz, T. Hocker, B. Much, M. Prestat, D. Wiedenmann, U. Vogt, P. Holtappels, J. Sfeir, A. Mai, T. Graule, J. Power Sources 196 (2010) 1279–1294.

[15] J. Sehested, J. Catal. 217 (2003) 417–426.

[16] J. Sehested, J. A. Gelten, I. N. Remediakis, H. Bengaard, J. K. Norskov, J. Catal. 223 (2004) 432–443.

[17] H. Sumi, R. Kishida, J.-Y. Kim, H. Muroyama, T. Matsui, K. Eguchi, J. Electrochem. Soc. 157 (2010) B1747–B1752.

[18] D. G. Ivey, E. Brightman, N. Brandon, J. Power Sources 195 (2010) 6301–6311.

[19] Y. Liu, C. Jiao, Solid State Ionics 176 (2005) 435–442.

[20] Y. C. Wu, J. G. Duh, J. Mater. Sci. Lett. 9 (1990) 583–586.

[21] T. Yamane, Y. Minamino, K. Hirao, H. Ohnishi, J. Mater. Sci. 21 (1986) 4227–4232.

[22] Q. Jeangros, A. Faes, J. Wagner, T. Hansen, U. Aschauer, J. V. herle, A. Hessler-Wyser, R. Dunin-Borkowski, Acta. Mater. 58 (2010) 4578–4589.

[23] S. M. Schnurre, J. Grobner, R. Schmid-Fetzer, J. Non-Cryst. Solids 336 (2004) 1–25.

[24] F. T. Ferguson, J. A. Nuth, J. Chem. Eng. Data 53 (2008) 2824–2832.

[25] E. Garcia, J. M. Guimaraes., P. Miranzo, M. Osendi, C. Cojocaru, Y. Wang, C. Moreau, R. Lima, J. Therm. Spray Tech. 20 (2011) 83–91.

[26] R. A. Eppler, J. Am. Ceram. Soc. 53 (1979) 457–462.

[27] K. M. Trappen, R. A. Eppler, J. Am. Ceram. Soc. 72 (1989) 882–885.

[28] I. R. Gibson, G. P. Dransfield, J. T. S. Irvine, J. Eur. Ceram. Soc. 18 (1998) 661–667.

[29] C. M. S. Rodrigues, J. A. Labrincha, F. M. B. Marques, J. Eur. Ceram. Soc. 18 (1998) 95–104.

[30] B. Butz, R. Schneider, D. Gerthsen, M. Schowalter, A. Rosenauer, Acta. Mater. 57 (2009) 5480–5490.

[31] S. P. S. Badwal, N. Nardella, Appl. Phys. A 49 (1989) 13–24.

[32] T. Sato, M. Shimada, J. Am. Ceram. Soc. 68 (1985) 356–356.

[33] V. Marcel, B. H. Anja, G. Ludwig, W. Jurgen, G. B. Wolfgang, J. Electrochem. Soc. 156 (2009) B663–B672.

[34] W. G. Bessler, J. Warnatz, D. G. Goodwin, Solid State Ionics 177 (2007) 3371–3383.

[35] K. V. Jensen, S. Primdahl, I. Chorkendorff, M. Mogensen, Solid State Ionics 144 (2001) 197–209.

[36] A. Ehn, J. Hogh, M. Graczyk, K. Norrman, L. Montelius, M. Linne, M. Mogensen, J. Electrochem. Soc. 157 (2010) B1588–B1596.

[37] J. Sehested, J. A. Gelten, S. Helveg, Appl. Catal A 309 (2006) 237–246.

[38] C. V. Bockstae, In situ study of the formation and properties of Nickel silicides, Ph.D. thesis, University Gent, US, 2010.
.

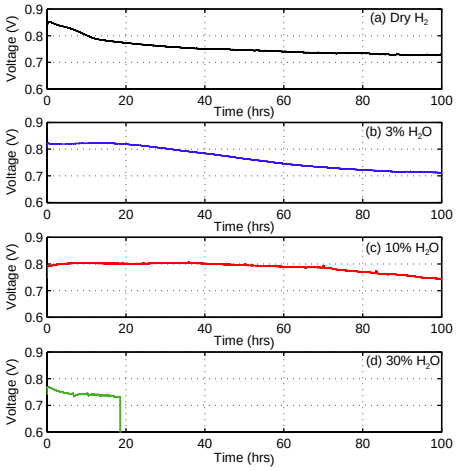

Figure 1: Cell performances measured in (a) dry, (b) 3%H_2O, (c) 10% H_2O and (d) 30% H_2O humidified hydrogen with galvanostatic method. (Anode-to-reference current density, 200 mAcm^{-2}, 100 hours).

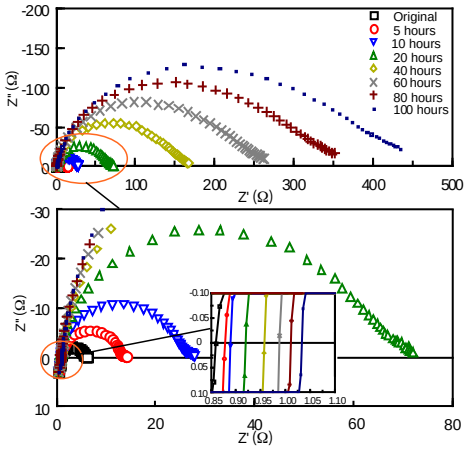

Figure 2: Anode-reference impedances after being kept at OCV for different periods in 3%H_2O hydrogen.

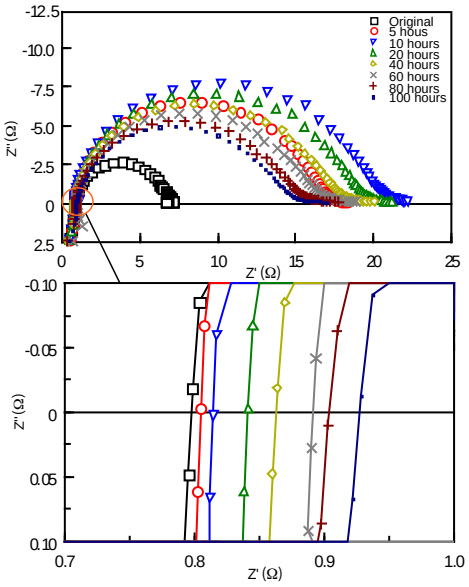

Figure 3: Anode-reference impedance after different time discharges in 3%H_2O hydrogen. (Current density, 200 $mAcm^{-2}$)

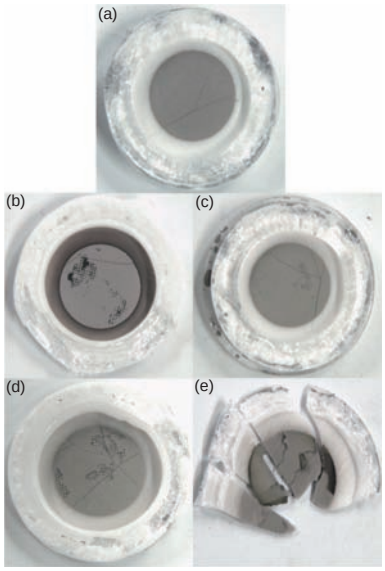

Figure 4: SEM images of the top views of anodes. (a) After reduction, (b)-(e) after discharge corresponding to Fig. 1 (a)-(d).

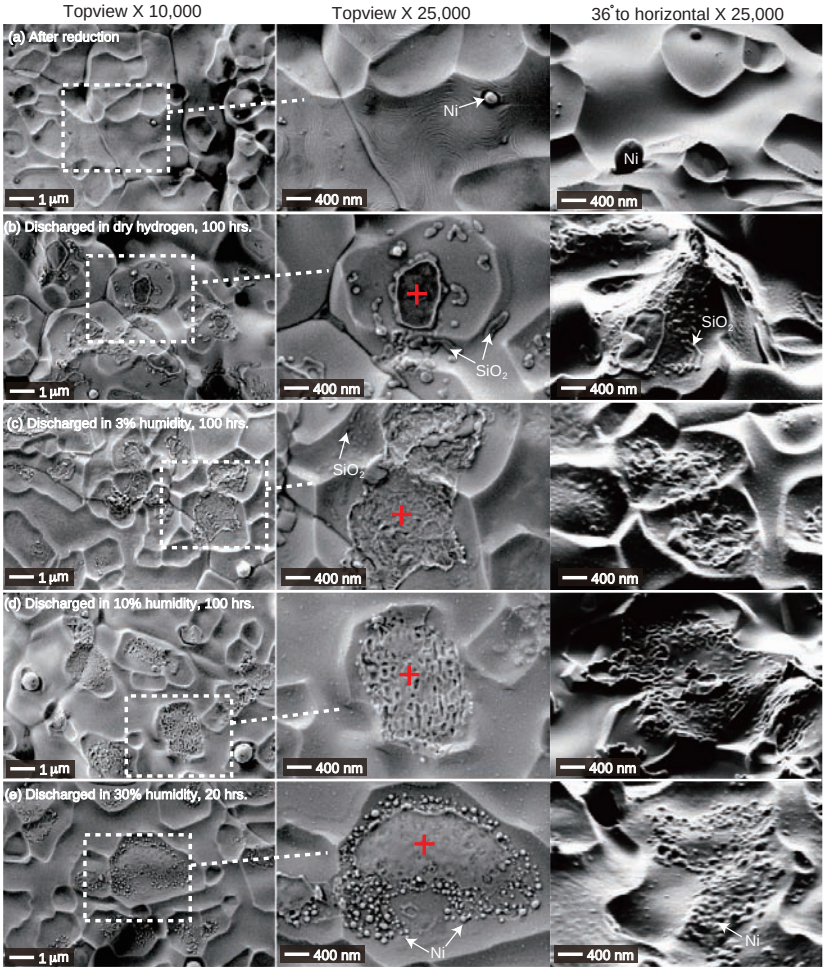

Figure 5: SEM images of YSZ-Ni interfaces (a) After reduction, (b)-(e) after discharge corresponding to Fig. 1 (a)-(d). (With Ni anode mechanically stripped off from YSZ surface.)

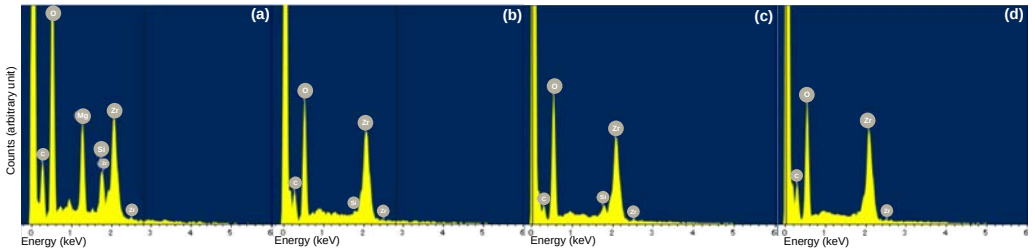

Figure 6: Point EDX spectra analysis corresponding to red cross symbols shown in Fig. 5 (b)-(e).

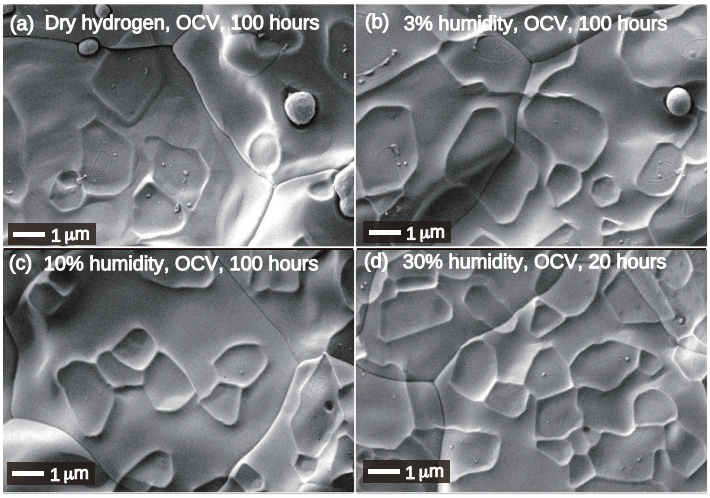

Figure 7: SEM images of the top views of YSZ-Ni interfaces after kept in OCV for 100 hours within (a) dry, (b) 3%H_2O, (c) 10% H_2O and (d) 30% H_2O humidified hydrogen. (With Ni anode mechanically stripped off from YSZ surface.)

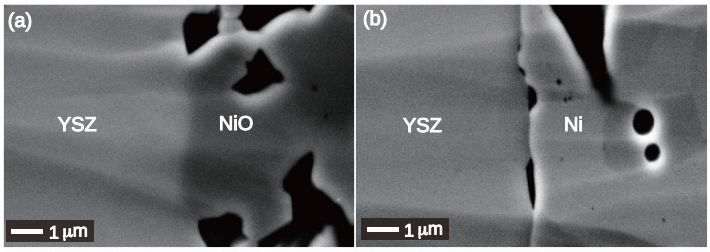

Figure 8: SEM images of (a) YSZ-NiO interface after sintering. (b) YSZ-Ni interface after reduction.

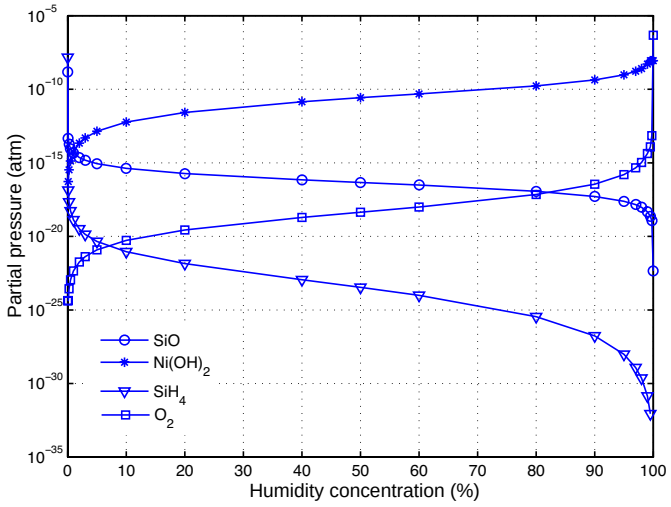

Figure 9: Partial pressure of gaseous phases versus humidity in hydrogen.

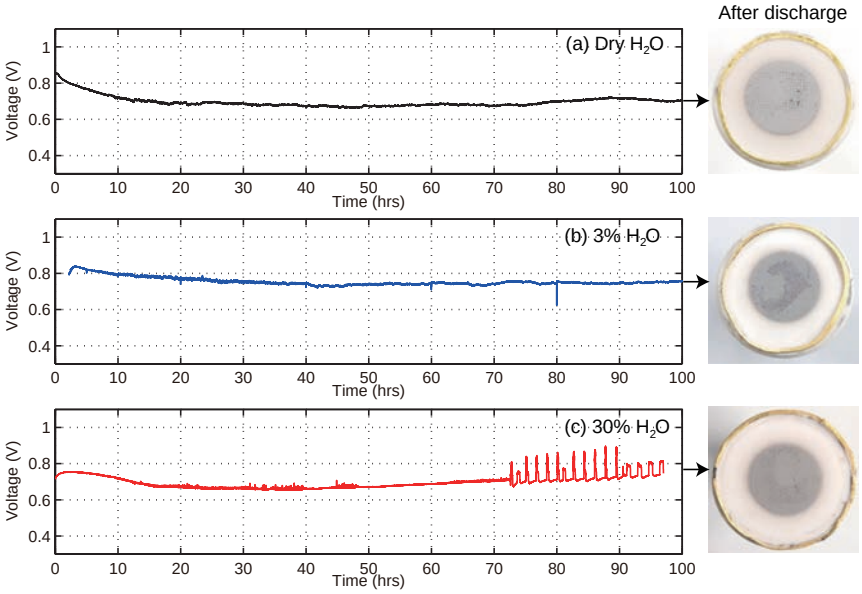

Figure 10: Cell performances measured in (a) dry, (b) 3%H_2O, and (c) 30% H_2O humidified hydrogen with galvanostatic method and images of anode side with gold seal. (Anode-to-reference current density, 200 mAcm^{-2}, 100 hours).

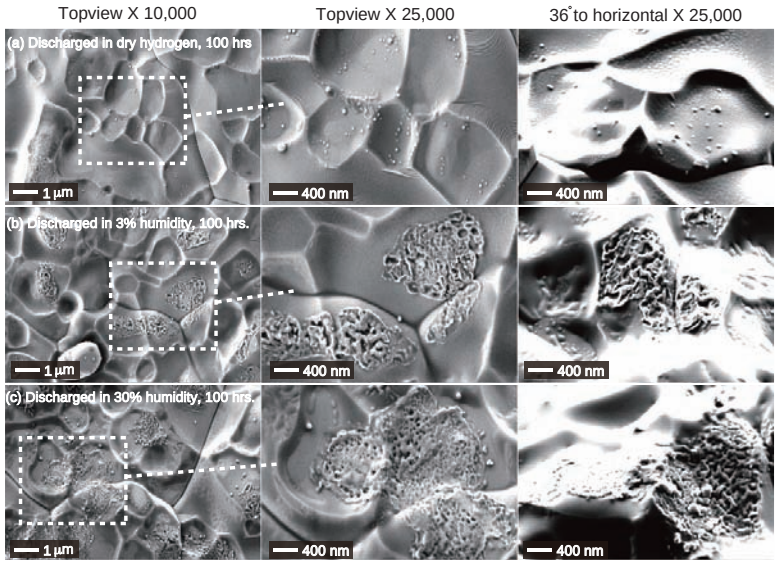

Figure 11: SEM images of YSZ-Ni interfaces (a)-(c) after discharge corresponding to Fig. 10 (a)-(c). (With Ni anode mechanically stripped off from YSZ surface)

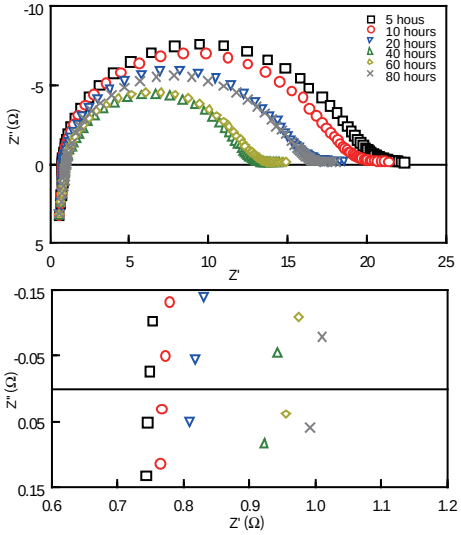

Figure 12: Anode-reference impedance after different time discharges in 3%H_2O hydrogen with gold ring for gas-sealing. (Current density, 200 mAcm^{-2})

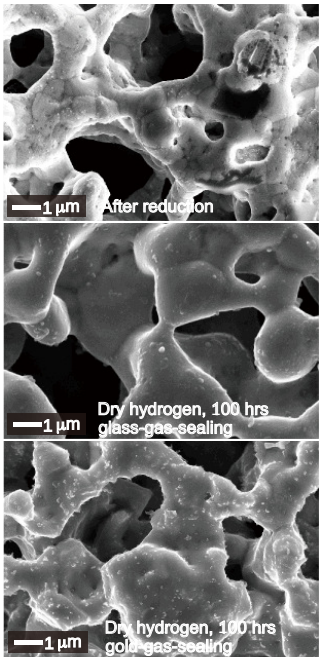

Figure 13: SEM images of Ni surfaces after (a) reduction and exposed in dry hydrogen for 100 hours with (b) glass seal and (c) gold seal.